**Smart Structures and Systems**, *Vol. 19, No. 5 (2017) 473-485*
DOI: https://doi.org/10.12989/sss.2017.19.5.473


# Effects of temperature on the ratcheting behavior of pressurized 90° elbow pipe under force controlled cyclic loading

Xiaohui Chen*[1,2], Xingang Wang[1] and Xu Chen[3a]

[1]*School of Control Engineering, Northeastern University, Qinhuangdao 066004, China.*
[2]*College of Mechanical Engineering, Yanshan University, Qinhuangdao, 066004, China.*
[3]*School of Chemical Engineering and Technology, Tianjin University, 300072, China*

*(Received March 19, 2016, Revised April 22, 2017, Accepted April 27, 2017)*

**Abstract.** Ratcheting behavior of 90° elbow piping subject to internal pressure 20 MPa and reversed bending 20 kN was investigated using experimental method. The maximum ratcheting strain was found in the circumferential direction of intrados. Ratcheting strain at flanks was also very large. Moreover, the effect of temperature on ratcheting strain of 90° elbow piping was studied through finite element analysis, and the results were compared with room condition (25°). The results revealed that ratcheting strain of 90° elbow piping increased with increasing temperature. Ratcheting boundary of 90° elbow piping was determined by Chaboche model combined with C-TDF method. The results revealed that there was no relationship between the dimensionless form of ratcheting boundary and temperature.

**Keywords:** elbow pipe; ratcheting strain; temperature; reversed bending; Chaboche model; ANSYS

## 1. Introduction

Piping and its various components, which were used to transport fluids at temperatures ranging from room to high temperatures, were important components of critical internal systems in industrial structures such as nuclear power plants and chemical installations. One particular frequently used component was the 90° elbow due to its flexibility when designing pipe systems. The 90° elbow had been difficult to properly analyze and model, due to its complex geometry. Elbows in piping systems were subjected to combinations of internal pressure, bending, and twisting cycles in addition to thermal fluctuations during their service life. Under these cyclic loading conditions, the elbow may exhibit significant accumulation of plastic strain, namely ratcheting effect. Ratcheting effect, a cyclic accumulation of inelastic deformation that occurs in materials subjected to a stress-controlled cyclic loading with non-zero mean stress. The ratcheting strain was a cyclic plastic strain accumulation process which took place in engineering components when they were subjected to asymmetrical cyclic stress and it largely depended on type of materials. Ratcheting deformation occurred in such a way that the hysteresis loops produced during subsequent cycles evolute towards higher plastic strain direction.

A systematic set of experiments of elbow components under combined loading of internal pressure and cyclic bending recording both the deformation and strain ratcheting is still scarce. In 2013, Chen *et al.* (2013) reviewed experimental and numerical studies on piping component mechanical ratcheting and thermal ratcheting, shakedown, fatigue failure responses. They concluded that the strain ratcheting in components has not been predicted well even by the advanced constitutive models. Hence, it was essential to critically evaluate the widely used and recently developed constitutive models against their simulation capability of component responses for determining the state-of-the-art constitutive modeling features and future model development needs. The results showed that the maximum ratcheting strain occurred mainly in the hoop direction at flanks. Hoop strain ratcheting was found at intrados for individual specimen. Ratcheting strain rate increases with the increase of bending loading level at a constant internal pressure. The results indicated that the initial rate of ratcheting is large and then it decreases with increasing cycles.

Few thermal ratcheting of 90° elbow pipe subjected to cyclic bending with and without internal pressure at high temperatures was reviewed in the reference (Chen *et al.* 2013). Heald and Kiss (1974) carried out an experiment on seven elbow pipings at room and high temperatures. The reason why they included internal pressure and high temperature was because they concerned with the ASME design code with respect to nuclear power plants and cyclic loading. From the results, it was clear that stainless steel was far more durable than carbon steel in terms of fatigue life. Griffith and Rodabaugh (1975) carried out 90° elbows test at high temperature (593.3℃) under force control mode. The results showed that the highest circumferential strain occurred at the flanks of the elbow. The measured circumferential and longitudinal strain was 80% and 36% higher than the calculated strain, respectively. These differences were attributed to the non-uniform wall

*Corresponding author, Ph.D.
E-mail: chenxh@neuq.edu.cn
[a] Ph.D.
E-mail: xchen@tju.edu.cn



ISSN: 1738-1584 (Print), 1738-1991 (Online)

thickness. Imazu *et al*. (1977) performed a high temperature experiment concerning creep of 304 stainless steel elbow pipe through experiment and finite element model using MARC. The results indicated that numerical results had some problems simulating the experimental values, which was attributed to a deviation of constitutive equations from the actual one as well as a neglect of the end effects. By means of experiment and finite element method, Bhandari *et al.* (1986) conducted 43 experiments on a stainless steel elbow with an initial crack and filled with liquid sodium in order to examine the fracture mechanics during cyclic loading. It was found out that the outer flaw's crack development agreed well with the model's predictions, while the inner flaw's crack development was proved to be hard to predict. Hilsenkopf *et al.* (1988) conducted experiments on ten ASME SA 106 grade B ferritic steel elbows and fifteen ASME TP 304L stainless steel elbows consisting of in-plane bending and out-of-plane bending.

These experiments were conducted at elevated temperatures subjected to in-plane or out-of-plane bending. The results indicated that the elevated temperature decreased elbow strength for in-plane closing and out-of-plane bending but did not have much effect on in-plane opening. In order to investigate the ratcheting effect under primary and thermal cyclic loads, thermal stress ratcheting behavior in elbows used in LMFBRs was studied by Ueda *et al*. (1990). The test results showed a progressive deformation of the elbow cross section which could be divided into transient ratcheting behavior followed by a steady state ratcheting behavior at each axial load. However, the transient ratcheting converged to zero ratcheting after about 15-30 cycles at the lower axial load. The authors concluded that the presence of transient ratcheting was due to stress redistribution and work-hardening of the elbow. Fenton (2015) tested both long and short radius elbows at room and high temperature under displacement controlled. Ratcheting behavior and low cyclic fatigue of a long radius elbow specimen in nuclear power plants at high temperature conditions was observed. It was found that the increasing temperature caused a dramatic decrease in peak load response. Observable load softening behavior was also presented. Using the load response to determine fatigue life, it was also apparent that the increased temperature greatly reduced the fatigue life of the elbow. Such testing is limited by data obtained during experiments.

Ratcheting strain of 90° elbow pipe was also studied by experiments and finite element analysis after 2013. For example, Varelis *et al*. (2013, 2014) compared the mechanical behavior of steel process piping elbows subjected to in-plane cyclic bending with or without internal pressure through experiment and numerical simulation. The results concluded that the numerical results of pipe elbows were in good agreement with experimental results in terms of both load–displacement curves and local strain ranges. Varelis *et al*. (2013) found the fatigue curve of the specimens to be quasi-linear on log–log scale, in terms of both the end-displacement range and the strain range at the crack location. The above results have been compared with ASME B31.3 and EN 13480-3 design standards for occasional loading conditions, illustrating the conservativeness of the relevant provisions especially for predicting the maximum bending moment of the elbow. Varelis *et al.* (2014) proposed a simple and efficient fatigue analysis methodology capable of predicting the fatigue life of specific elbows under strong in-plane cyclic bending conditions in the presence of internal pressure loads. Ratcheting deformation in elbow pipe made of Z2CND18.12N stainless steel with local wall thinning subjected to constant internal pressure and reversed in-plane bending was investigated by Shi *et al.* (2013) under force control through three-dimensional elastic-plastic analyses using ANSYS incorporated with Chaboche (Chaboche *et al*. 1979, 1986) and Chen-Jiao-Kim (CJK) kinematic hardening models (Chen *et al*. 2005). The results indicated that the simulated results incorporated with CJK model for the ratcheting of elbows were in reasonable agreement with experimental data. The ratcheting boundary was determined by evaluating variations in the plastic strain increment with CJK model. Moreover, the effects of depth and location of local wall thinning on the ratcheting response were discussed with CJK model. In order to obtain ratcheting strain at the inner surface of elbow, Gudur (2013) investigated the ratcheting behavior of typical nuclear power plant elbow piping by means of 3-D non-linear finite element analyses incorporating multilinear kinematic hardening law and Chaboche model. Results indicated that compared to the multilinear kinematic hardening law, Chaboche model was more appropriate to characterize the experimental behavior. Zakavi and his co-workers (2014) studied ratcheting behavior of carbon steel pressurized elbow piping subjected to internal pressure and dynamic in-plane or out-of-plane bending moment through finite element analysis incorporating the nonlinear kinematic hardening model. For dynamic in-plane cyclic bending, the results concluded that hoop strain ratcheting rate of experiment and finite element analysis was near in all cases that $M/M_l \leq 1$. For dynamic out-plane cyclic bending, the results concluded that the direction of maximum strain was about 45° between the hoop and axial directions. The finite element method overestimated the experimental data (Yahiaoui *et al.* 1996). Chen *et al*. (2015, 2016) studied ratcheting strain of Z2CND18.12N stainless steel pressurized straight pipe and 90° elbow pipe with and without local wall thinning under loading-controlled mode through experiments and finite element analysis combined with non-linear kinematic hardening model. The predicted results of Chen-Jiao-Kim model were in well agreement with experimental results. The effect of different local wall thinning on ratcheting strain was different. Hassan and his co-worker (2015) investigated low-cycle fatigue and ratcheting responses of elbows through experimental and analytical methods under displacement control. All elbow specimens tested were subjected to reversed bending with and without internal pressure. Seven different constitutive models were used to simulate ratcheting responses of straight pipe and 90° elbow pipe remains. It was found that the ratcheting responses simulated by these constitutive models remains to be a challenging problem. Karamanos (2016) summarized the mechanical behavior of steel pipe

Table 1 Chemical composition of Z2CND18.12N steel (in wt%)

| Constituent | C | Cr | Ni | Si | Mn | S | P | V | Mo | N |
|---|---|---|---|---|---|---|---|---|---|---|
| Content | 0.03 | 17.14 | 11.45 | 0.37 | 1.64 | 0.001 | 0.03 | 0.087 | 2.43 | 0.064 |

(elbows) based on analytical solutions, numerical results and experimental data. The main feature of pipe bends under bending loading (in-plane and out-of-plane) was cross-sectional ovalization, which influenced bending capacity and was affected by internal pressure level. Bends subjected to cyclic in-plane bending exhibited fatigue damage, leading to base metal cracking at the elbow flanks.

Note that from the above references, the researchers did not choose comparable tests between room and high temperatures, so it was difficult to draw conclusions on the effect of temperature. Therefore, the novelty of the paper was in the following three points. Firstly, ratcheting behavior at room temperature (25°) of pressurized Z2CND18.12N austenitic stainless steel 90° elbow pipe subjected to in-plane reversed bending through experiments was studied in this paper. Secondly, the effect of temperature on ratcheting behavior of pressurized 90° elbow pipe subjected to in-plane reversed bending was studied by means of finite element analysis. Finally, Ratcheting boundary of pressurized 90° elbow pipe was calculated by Chaboche kinematic hardening which combined with C-TDF (Committee of Three Dimensional Finite Element Stress Evaluation).

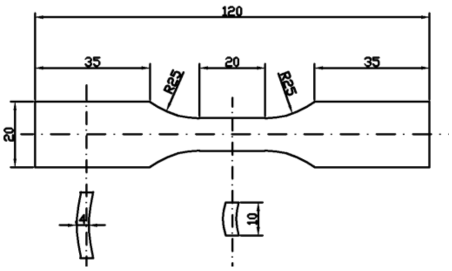


(a) Test specimen

(b) Experimental apparatus

Fig. 1 Plate tension specimen and test apparatus

## 2. Materials and experiments

The 90°elbow which was used as the auxiliary piping of the primary coolant circuit for pressurized water reactor, were made of austenitic stainless steel Z2CND18.12N. Chaboche model was used to predict ratcheting behavior and ratcheting boundary, mechanical properties and uniaxial ratcheting strain of austenitic stainless steel Z2CND18.12N should be first studied. Because the parameters of Chaboche model were determined by means of mechanical properties and uniaxial ratcheting strain of austenitic stainless steel Z2CND18.12N. Chemical composition of Z2CND18.12N steel was listed in Table 1.

Fig. 1 show the geometry of standard dumbbell-shaped test specimen which was machined along the axial direction of straight pipe. Ratcheting tests were conducted on Letry electro-hydraulic servo fatigue test machine. A 12.5 mm gauge length extensometer was used to measure ratcheting strain which was recorded by a computerized data acquisition system. Force controlled tests and displacement controlled tests were conducted. Loading waveform was triangular wave.

## 3. Results and discussion

### *3.1 Uniaxial tension*

In order to obtain the basic mechanical properties of austenitic stainless steel Z2CND18.12N, uniaxial tension tests under different temperatures were conducted on Letry Electro-hydraulic Servo Fatigue Test Machine. Uniaxial stress-strian curves under different temperatures were shown in Fig. 2 Elastic modulus was determined by linear fitting based on least square method. A parallel line, which was in parallel with linear part of uniaxial tension curve, passed through point (0.2%, 0). Yield stress was the cross point $\sigma_{0.2}$ of this parallel line with uniaxial stress-strain curve. Table 2 shows the elastic modulus and yield stress of austenitic stainless steel Z2CND18.12N under different temperatures.

### *3.2 Uniaxial ratcheting behavior*

The experimental result at room temperature under mean stress of 125 MPa and stress amplitude of 200 MPa was taken as an example. The control mode was triangular wave under force control with the stress rate of 100MP/s, as shown in Fig. 3(a). The stress-strain response shown in Fig. 3(b) indicated that the hysteresis loop at initial cycles was not closed.

This phenomenon became less obvious with the increase of number of cycles, corresponding to the accumulation of ratcheting strain. Fig. 3(c) indicated that ratcheting strain rate at initial cycles was large, which was attributed to the open hysteresis loop. Ratcheting strain rate trended toward a small steady value, namely $1.19\times10^{-6}$/s, as shown inFig. 3(d).. Not closed hysteresis loop of stress and strain was not obvious at this time.

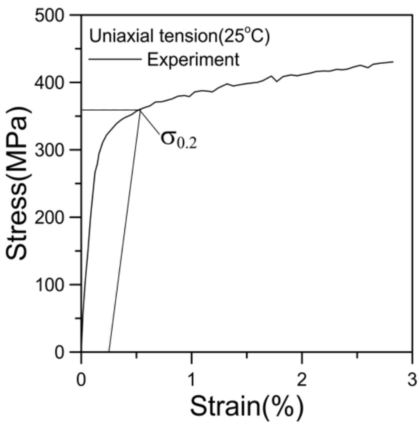


(a) 25℃

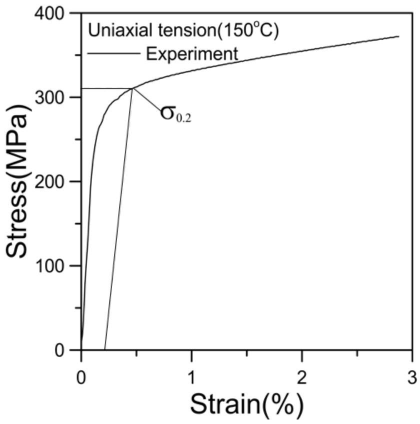


(b) 150℃

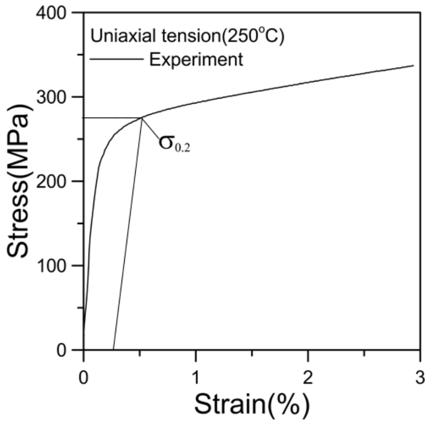


(c) 250℃

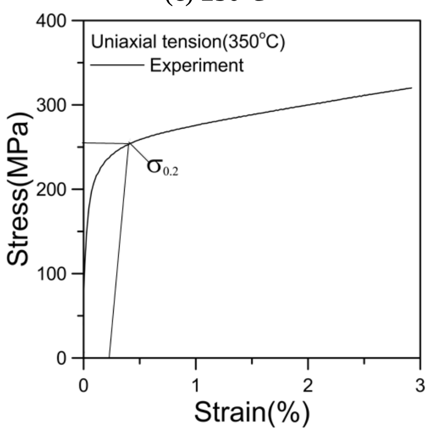


(d) 350℃

Fig. 2 Monotonic tensile curve at different temperatures

Table 2 Mechanical properties of Z2CND18.12N steel at different temperatures

| Temperature (℃) | Elastic modulus $E$, GPa | Tangent modulus $E_T$, GPa | Yield limit $\sigma_y$, Mpa |
|---|---|---|---|
| 25 | 195 | 1.712 | 366 |
| 150 | 180 | 1.755 | 324 |
| 250 | 170 | 1.887 | 283 |
| 350 | 165 | 1.946 | 265 |

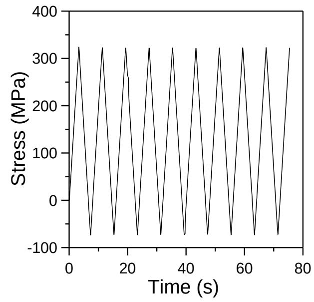


(a) Stress control diagram

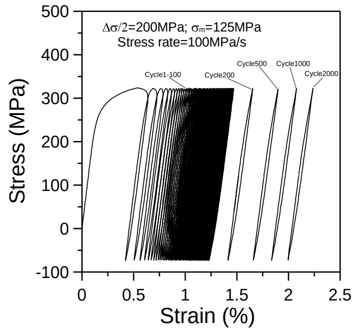


(b) Stress-strain relationship

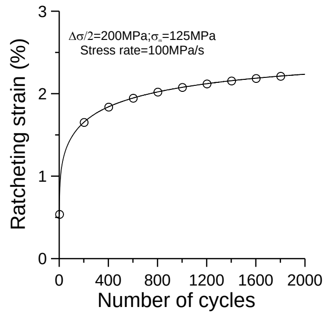


(c) Ratcheting strain

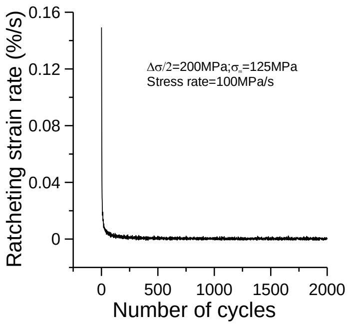


(d) Ratcheting strain rate

Fig. 3Uniaxial ratcheting test at 25°

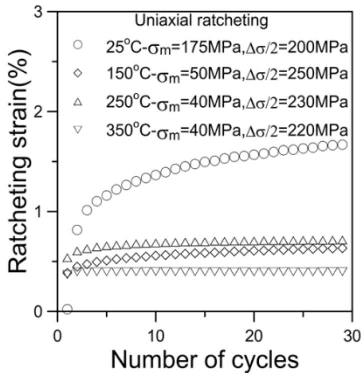


Fig. 4 The evolution of uniaxial ratcheting strain under different temperatures

Fig. 4 compared the evolution of uniaxial ratcheting strain of austenitic stainless steel Z2CND18.12N under different temperatures. Uniaxial ratcheting strain in Fig. 4 was at different mean stress and different stress amplitude, so these uniaxial ratcheting strains were no comparable. They were only used to determine the parameters of Chaboche model under different temperatures in section 5.3.

## 4. Ratcheting behavior of 90°elbow pipe under cyclic bending and constant internal pressure

### *4.1 Experimental setup*

The top connecting block of the elbow specimen was pin connected to the loading bar on the cross clamp of the Letry electro-hydraulic servo fatigue test machine. The bottom connecting block was connected by pin connection to the hydraulic actuator through which the force or displacement controlled loading was applied. Fig. 5 both an image of a 90° elbow test specimen setup at room temperature in the MTS as well as a line detail of a test specimen that also displayed the boundary conditions. So far, ratcheting strain tests of pressurized elbow specimen at high temperature have not been carried out. In the future, we will conduct ratcheting strain tests of pressurized elbow or straight pipe at high temperature. In this study, ratcheting behavior of pressurized elbow pipe at high temperature was simulated by finite element software ANSYS with Chaboche model, and was compared with that at room temperature (25°). The location of the critical point of 90° elbow pipe such as flank, intrados and extrados was given in Fig. 5.

### *4.2 Experimental results*

Fig. 6 showed loading spectrum of 90° elbow specimen. The fluctuation range of internal pressure was very small, as shown in Fig. 6(a). Therefore, the effect of the fluctuation range of internal pressure on ratcheting behavior can be ignored. Fig. 6(b) gave loading spectrum of reversed bending which was applied by triangular waveform, namely force control.

(a) Set up of experimental apparatus

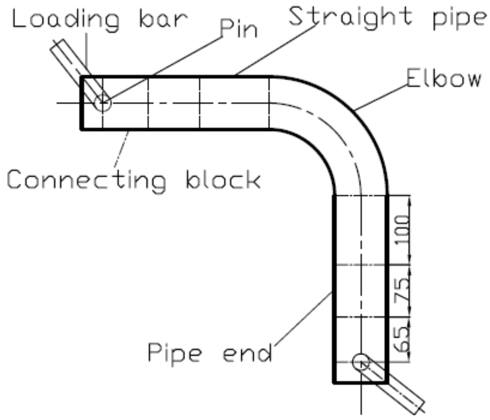


(b) Sketch of experimental specimen

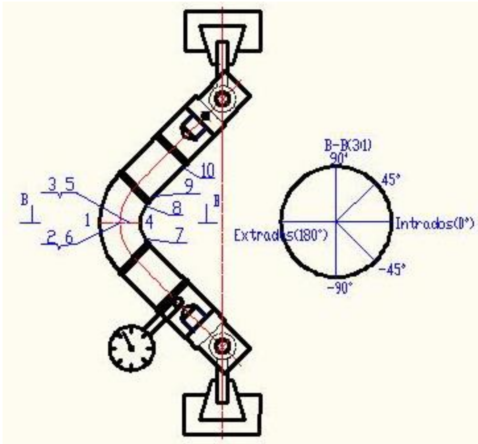


(c) Sketch of experimental apparatus

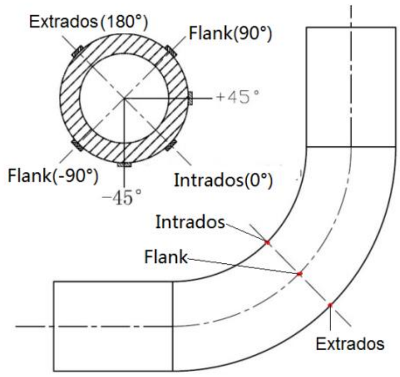


(d) Gauge distribution

Fig. 5 Sketch of experimental apparatus

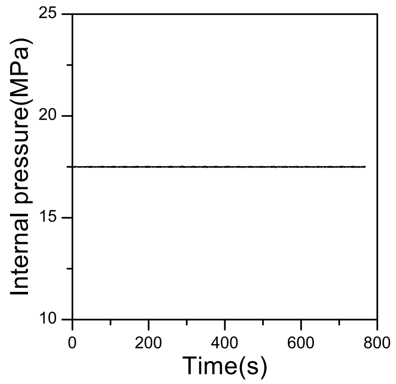


(a) Internal pressure versus time

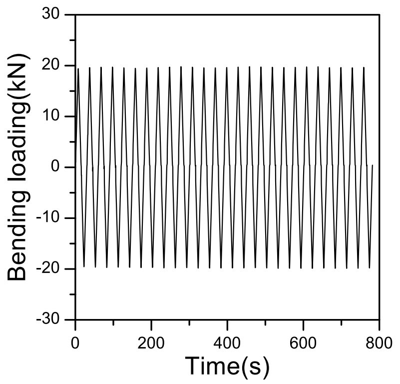


(b) Bending loading versus time

Fig. 6 Loading spectrum

Using the ratcheting tests of 90° elbow piping at 25° as an example, the curve of axial strain versus hoop strain at flanks and intrados of 90°elbow piping subjected to 17.5 MPa internal pressure and 20 kN reversed bending was shown in Fig. 7. It was found that hoop ratcheting strain was larger than that of axial direction. Ratcheting strain at intrados was larger than that of flank.

Fig. 8 indicated the evolution history of hoop and axial strain at flanks and intrados of 90°elbow piping subjected to 17.5 MPa internal pressure and 20 kN reversed bending. It was found that hoop strain was larger than axial strain. In other words, ratcheting strain occurred mainly at hoop direction. In general, Chen *et al.* (2013) summarized that ratcheting strain mainly occurred in the circumferential direction of 90° elbow piping at flanks. Sometime the maximum ratcheting strain also occurred at intrados. Ratcheting behavior of 90°elbow piping at flanks, intrados, extrados and 45° position at midway between flanks and intrados was studied by many scholars. In this study, maximum ratcheting strain occurred at intrados.

The curves of axial and hoop ratcheting strain at flanks, intrados and extrados versus the number of cycles were shown in Fig. 9. It was found that ratcheting strain mainly occurred in the circumferential direction of 90°elbow piping. Ratcheting strain at intrados was larger than that at flanks. In other words, maximum ratcheting strain occurred at intrados. Ratcheting strain at extrados was very small, even no at extrados.

Hoop ratcheting strain rate decreased with the number of cycles, but shakedown phenomenon was not seen.

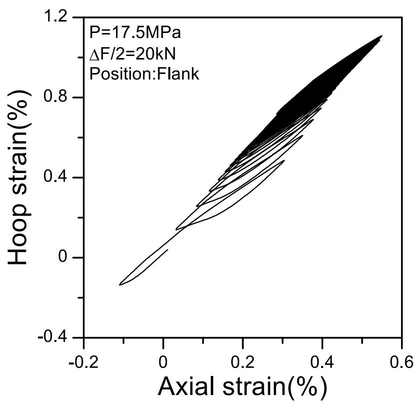


(a) At flank

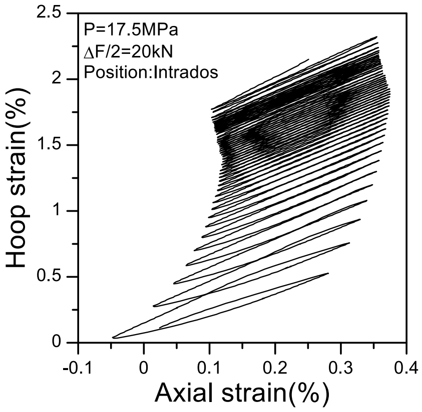


(b) At intrados

Fig. 7 Relationship between hoop strain and axial strain

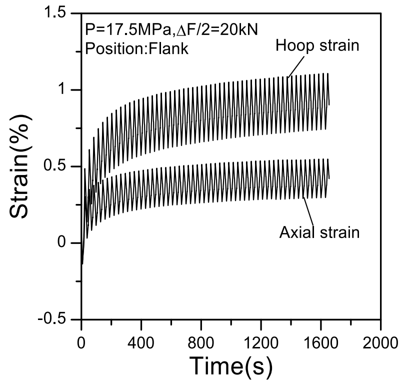


(a) At flank

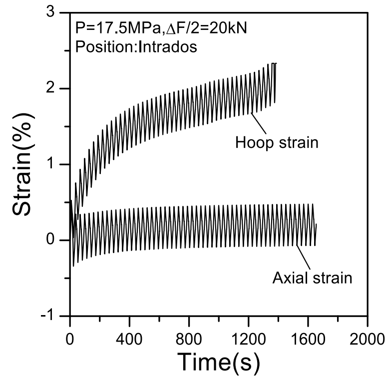


(b) At intrados

Fig. 8 Strain history

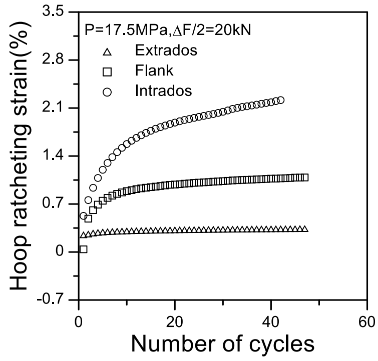


(a) Hoop ratcheting strain

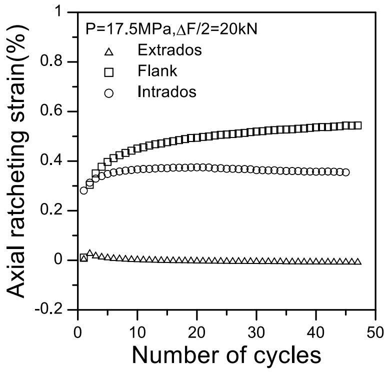


(b) Axial ratcheting strain

Fig. 9 Ratcheting strain

## 5. Finite element model

### 5.1 Geometric model

The 90° elbow specimen and loading prescribed was doubly symmetric. The elbow and pipe considered in this study was thin shell structure. Hence, the elbow was modeled with Shell43 elements in ANSYS9.0. Using the double symmetry of the structure as well as considering the symmetric loading condition, only one quarter of the specimen was modeled for finite element simulations, as shown in Fig. 10(a). Consequently only half of the loading was prescribed for force controlled experimental simulations. The boundary conditions of the model came from the double symmetry of specimen and loading. The inside surface of elbow pipe was applied by internal pressure, one point on the symmetric cross-section of pipe end was applied by reversed bending, as given in Fig. 10(b).

The straight pipe end of the elbow specimen was sealed with shell elements with high modulus of rigidity. The lug end was modeled as a rigid plate with high modulus of rigidity shell elements. The loading were prescribed at the lug end shown in Fig. 5(a). The quarter of the elbow specimen was modeled with uniform thickness for the pipe and elbow. In fact, the thickness of the elbow and the pipe is not uniform; the assumption of uniform thickness was still an approximation of the structure. The pipe dimensions usually were circular in shape, but 90° elbow dimensions usually were elliptical as also observed from the measured diameters.

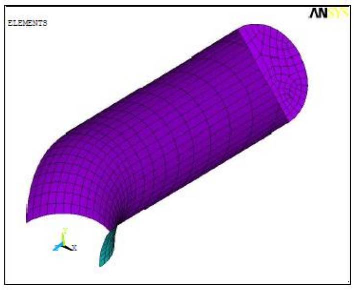


(a) Finite element meshs

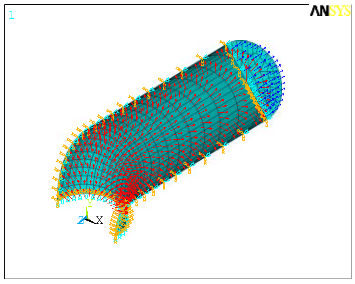


(b) Boundary conditions and load

Fig. 10 Finite element meshs and boundary conditions and load

### 5.2 Constitutive modeling

The nonlinear kinematic hardening rule was first proposed by Armstrong and Frederick (2007). Nonlinearities were given as a recall term in the Prager rule. The kinematic hardening plasticity models were proposed to model the inelastic behavior of materials that were subjected to repeated loading. The nonlinearities were given as a recall term. So that the transformation of yield surface in the stress space was different during loading and unloading. This was done by assuming different hardening modulus in loading and unloading conditions. The yield function for time independent plasticity using the von-Mises yield criterion, was expressed as following.

$$f = \left[\frac{3}{2}(\mathbf{s}-\mathbf{a}):(\mathbf{s}-\mathbf{a})\right]^{1/2} - k = 0 \tag{1}$$

where, $\mathbf{s}$ was the deviatoric stress tensor, $\mathbf{a}$ was the deviatoric back stress tensor, $k$ was the initial size of the yield surface, and denoted the von-Mises distance in the deviatoric stress space.

Chaboche *et al.* (1979, 1986) proposed that when three or more Armstrong-Frederick rules were superimposed (Abbr. CH3 model) as follows.

$$d\boldsymbol{\alpha} = \sum_{i=1}^{M} d\boldsymbol{\alpha}_i \quad (i=1,2,3) \tag{2}$$

$$d\boldsymbol{\alpha}_i = \frac{2}{3} r_i \gamma_i d\boldsymbol{\varepsilon}_p - \gamma_i \boldsymbol{\alpha}_i dp \quad (i=1,2,3) \tag{3}$$

where $r_i$ and $\gamma_i$ were the material dependent coefficients. $d\boldsymbol{\varepsilon}_p$ was equivalent plastic strain rate, $dp$ was the increment of accumulated plastic strain.

$$dp = \left[\frac{2}{3} d\boldsymbol{\varepsilon}_p \bullet d\boldsymbol{\varepsilon}_p\right]^{\frac{1}{2}} \tag{4}$$

The normality hypothesis and the consistency condition $df = 0$ led to the expression for the plastic strain rate (Lemaitre and Chaboche 1994).

$$d\boldsymbol{\varepsilon}^p = d\lambda \frac{\partial f}{\partial \boldsymbol{\sigma}} = \frac{H(f)}{h} \left\langle \frac{\partial f}{\partial \boldsymbol{\sigma}} : d\boldsymbol{\sigma} \right\rangle \frac{\partial f}{\partial \boldsymbol{\sigma}} \tag{5}$$

where, $d\lambda$ was the plastic multiplier, $\frac{\partial f}{\partial \boldsymbol{\sigma}}$ was the direction of the plastic strain increment, $h$ was the hardening modulus, $H$ denoted the Heaviside step function: $H(f)=0$ if $f<0$, $H(f)=1$ if $f \geq 0$ and the symbol $\langle \ \rangle$ denoted the MacCauley bracket, i.e., $\langle u \rangle = (u + |u|)/2$.

The hardening modulus $h$ became

$$h = \sum_{i=1}^{M} \left( \gamma_i r_i - \frac{3}{2} \gamma_i \boldsymbol{\alpha}_i \frac{\mathbf{s}_i - \mathbf{a}_i}{k} \right) \qquad (i = 1,2,3) \tag{6}$$

In the case of tension-compression, the criterion and the equations of flow and hardening can be expressed in the form (Lemaitre and Chaboche 1994)

$$f = |\boldsymbol{\sigma} - \boldsymbol{\alpha}| - k = 0 \tag{7}$$

where, $\boldsymbol{\sigma}$ was the stress tensor, $\boldsymbol{\alpha}$ was the back stress tensor, $k$ was the initial size of the yield surface.

$$d\boldsymbol{\varepsilon}^p = \frac{1}{h} \left\langle \frac{\boldsymbol{\sigma} - \boldsymbol{\alpha}}{k} d\boldsymbol{\sigma} \right\rangle \frac{\boldsymbol{\sigma} - \boldsymbol{\alpha}}{k} = \frac{d\boldsymbol{\sigma}}{h} \tag{8}$$

$$d\boldsymbol{\alpha} = C d\boldsymbol{\varepsilon}_p - \gamma \boldsymbol{\alpha} dp \tag{9}$$

$$h = C - \gamma \boldsymbol{\alpha} Sgn(\boldsymbol{\sigma} - \boldsymbol{\alpha}) \tag{10}$$

The evolution equation of hardening can be integrated analytically to give

$$\boldsymbol{\alpha} = \nu \frac{C}{\gamma} - \left( \boldsymbol{\alpha}_0 - \nu \frac{C}{\gamma} \right) \exp\left[ -\nu\gamma \left( \boldsymbol{\varepsilon}_p - \boldsymbol{\varepsilon}_{p0} \right) \right] \tag{11}$$

where $\nu = \pm 1$ according to the direction of flow, and $\boldsymbol{\varepsilon}_{p0}$ and $\boldsymbol{\alpha}_0$ were the initial values.

The parameters of Chaboche model were determined through the stress-strain and uniaxial ratcheting responses. It still overpredicted multiaxial ratcheting simulation (Bari and Hassan 2000). But the Chaboche model was available from finite element software ANSYS, and compared to the advanced constitutive models.

### *5.3 Model parameter determination*

In general, Chaboche model, which can predict better ratcheting strain of material or a component / structural, was available in ANSYS software. The parameters of Chaboche model under different temperatures were determined by uniaxial tension and uniaxial ratcheting experimental data, respectively. Fig. 11(a) gave uniaxial tension curve at 25℃, 150℃, 250℃ and 350℃. It was shown in Fig. 11(a) that the relationship between stress and strain was variational with the increase of temperature. That is, yield stress decreased with the increase of temperature. Uniaxial ratcheting data under different temperatures was shown in Fig. 11(c)-(f), respectively.

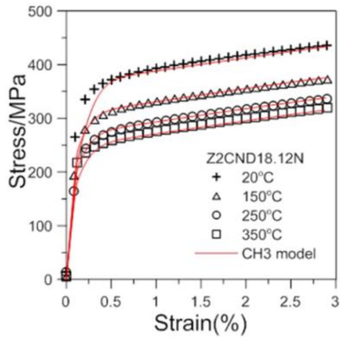


(a) Uniaixal tension

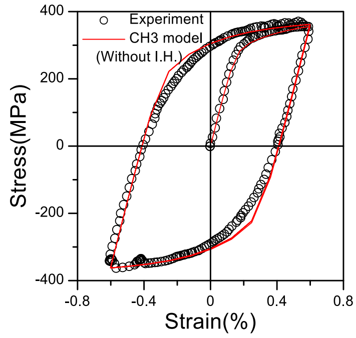


(b) Strain cycles at 25℃

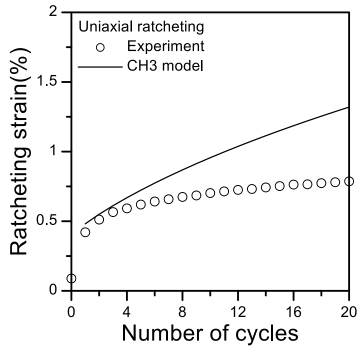


(c) uniaxial ratcheting strain under 25℃

Continued-

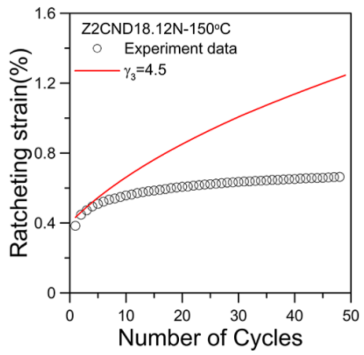


(d) uniaxial ratcheting strain under 150°C

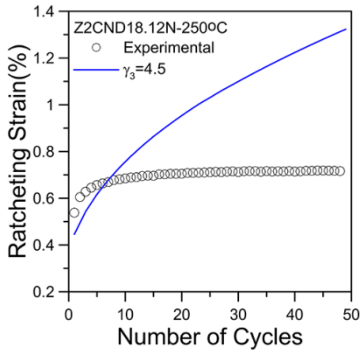


(e) uniaxial ratcheting strain under 250°C

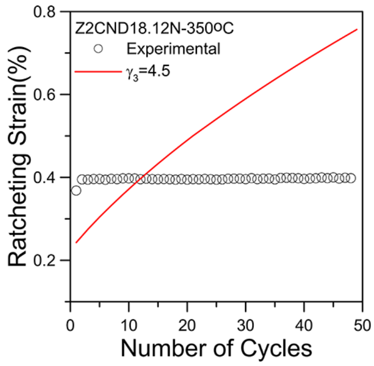


(f) uniaxial ratcheting strain under 350°C

Fig. 11 Parameter determination for the CH3 model (M=3) with and without isotropic hardening rule

Table 3 Parameter determination for the CH3 model (M=3) isotropic hardening rule under different temperatures

| Temperature (℃) | $E$ (GPa) | $\sigma_y^0$ (MPa) | $C_{1\text{-}3}$ (MPa) | $\gamma_{1\text{-}3}$ |
|---|---|---|---|---|
| 25 | 195 | 100 | 4.0×10$^6$、1.5×10$^5$、2500 | 4.0×10$^4$、870、4.5 |
| 150 | 180 | 82 | 4.0×10$^6$、1.1×10$^5$、2500 | 4.0×10$^4$、900、4.5 |
| 250 | 170 | 76.7 | 4.0×10$^6$、0.9×10$^5$、2500 | 4.0×10$^4$、900、4.5 |
| 350 | 165 | 60 | 4.0×10$^6$、0.9×10$^5$、2500 | 4.0×10$^4$、950、4.5 |

## 6. Structural simulation for force controlled tests

### *6.1 Simulation results*

#### *6.1.1 25℃ temperature*

With simulation results at room temperature of 90° elbow piping for 17.5 MPa internal pressure and 20 kN reversed bending, equivalent plastic strain contour in 10 cycles was shown in Fig. 14 using Chaboche model. It was found in Fig. 12(a) that the maximum equivalent plastic strain at the outside surface occurred at flanks, and the equivalent plastic strain at 45° position at midway between flank and intrados of the outside surface was also larger. Taking flanks and 45° position at midway between flank and intrados on the XZ symmetry plane as the center, the equivalent plastic strain extended along the meridional and circumferential direction. For the inside surface, Fig. 12(b) indicated the maximum equivalent plastic strain at intrados, and the equivalent plastic strain at flanks was also large. Using flanks and intrados on the XZ symmetry plane as the center, the equivalent plastic strain extended along the meridional and circumferential direction.

Fig. 13 showed that ratcheting strain occurred at flanks, intrados and extrados of 90° elbow piping subjected to 17.5 MPa internal pressure and 20 kN reversed bending, ratcheting strain rate increased during the initial several cycles, and then decreased with number of cycles. Axial and circumferential ratcheting strains were shown in Fig. 13.

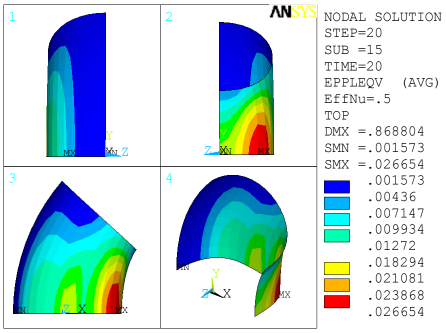


(a) Ratcheting strain of outside surface

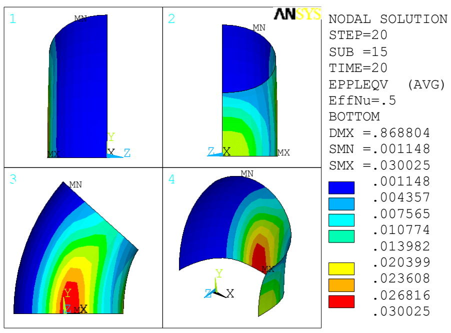


(b) Ratcheting strain of inside surface

Fig. 12 Ratcheting strain contour of pressurized elbow piping at 25°C subjected to cyclic bending loading after 10 cycles

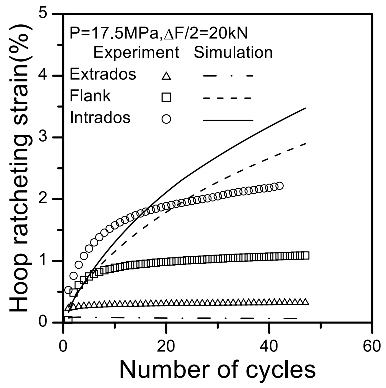


Fig. 13 Comparison of experiment data and predicted results of Chaboche model

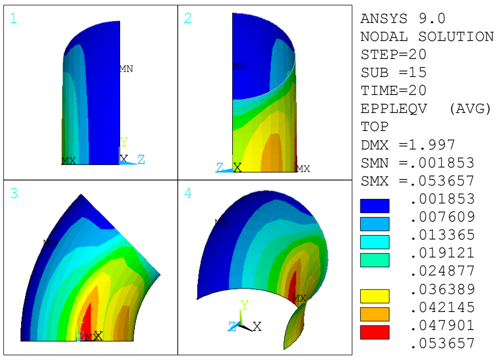


(a) Ratcheting strain of outside surface

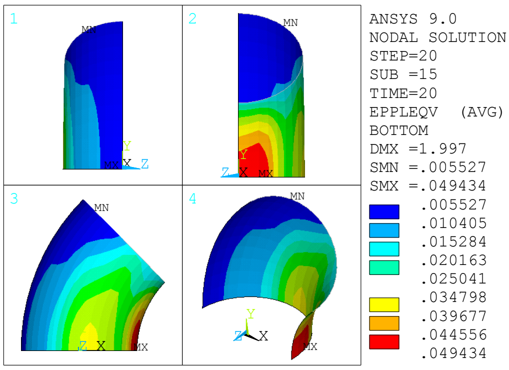


(b) Ratcheting strain of inside surface

Fig. 14 Ratcheting strain contour of pressurized elbow piping subjected to cyclic bending loading after 10 cycles

It was found that circumferential ratcheting strains at flanks, intrados and extrados of 90° elbow were larger than those of axial direction. In other words, ratcheting strain occurred mainly at circumferential direction. Chen *et al*. (2013) summarized that the circumferential ratcheting strains of 90° elbow piping subjected to internal pressure and reversed bending occurred at flanks or intrados. In general, maximum ratcheting strain of 90° elbow piping subjected to internal pressure and reversed bending occurred at flanks. Sometimes, ratcheting strain at intrados was maximum. In this study, maximum ratcheting strain at intrados of 90° elbow piping subjected to internal pressure and reversed bending was maximum.

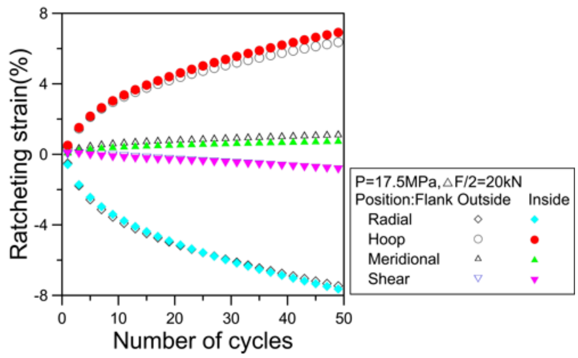


(a) At flank

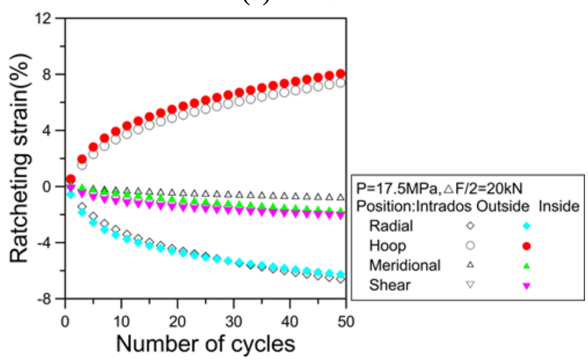


(b) At Intrados

Fig. 15 Ratcheting strain

### *6.1.2 250℃ temperature*

With simulation results at 250° of 90° elbow piping for 20MPa internal pressure and 20kN reversed bending, equivalent plastic strain contour in 10 cycles was shown in Fig. 14 using Chaboche model. It was found in Fig. 14(a) that the maximum equivalent plastic strain at the outside surface occurred at flanks, and the equivalent plastic strain at 45° position at midway between flank and intrados of the outside surface was also larger. Taking flanks and 45° position at midway between flank and intrados on the XZ symmetry plane as the center, the equivalent plastic strain extended along the meridional and circumferential direction. For the inside surface, Fig. 14(b) indicated the maximum equivalent plastic strain at intrados, and the equivalent plastic strain at flanks was also large. Using flanks and intrados on the XZ symmetry plane as the center, the equivalent plastic strain extended along the meridional and circumferential direction.

Fig. 15 compared ratcheting strain at flanks and intrados of all directions on the inside and outside surfaces. It was found that ratcheting strain occurred in the hoop direction, ratcheting strain in radial and shear direction was not obvious. The shape of the elbow cross section was shown in Fig. 16.

### *6.2 The effect of the temperature on ratcheting behavior*

Fig. 17 indicated the ratcheting strain at intrados, 45° position at midway between flank and intrados, flanks and extrados of pressurized elbow piping subjected to reversed bending at 25℃, 150℃, 250℃ and 350℃. Ratcheting strain of these positions increased with the increase of temperatures. It was found in Fig. 17 that ratcheting behavior at extrados was very small at room temperature (25℃). But ratcheting behavior at extrados was relative smaller at room temperature (25℃).

### *6.3 Ratcheting boundary determination*

Elasto–plastic finite element analysis with CH3 model and combined with C-TDF (Asada *et al.* 2002, Yamamoto *et al.* 2002) was used to determine ratcheting boundary in the study. One criterion of C-TDF is that 'Variations in equivalent plastic strain at the end of each cycle should have a decreasing trend and should become lower than the allowable limit of $10^{-4}$/cycle.' The number of cycles required to achieve this value was not specified, but usually 5 or 10 cycles were needed. The ratchetting rate was based on the values of the first 10 cycles. Applied internal pressure and cyclic bending loading were represented in the form of non-dimensional parameters X and Y with the following definitions (Chen *et al.* 2005, 2006) in order to understand the ratcheting behavior of pressurized pipes.

$$X = \frac{P}{P_{sy}} \tag{12}$$

where, $P_{sy}$ corresponded to the pressure value where the straight pipe with the same schedule yields at inner surface

$$P_{sy} = \frac{K^2\text{-}1}{K^2+1}\sigma_y \tag{13}$$

where, $K = r_o / r_i$, $r_o$ and $r_i$ were the outside radius and inside radius of pipe, respectively. $\sigma_y$ was yield stress

$$Y = \frac{\Delta F}{F_{sy}} \tag{14}$$

where, $F_{sy}$ corresponded to the bending loading where the straight pipe with the same schedule yields at outside surface

$$F_{sy} = \frac{\pi\left(r_o^4\text{-}r_i^4\right)\sigma_y}{4 r_o L_s \sin\left(\theta/2\right)} \tag{15}$$

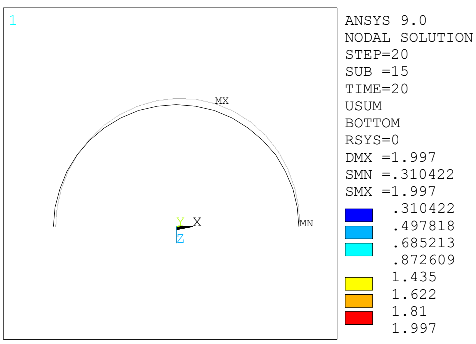


Fig. 16 Cross section deformation

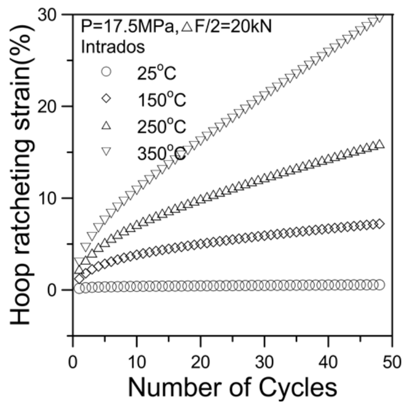


(a) At intrados

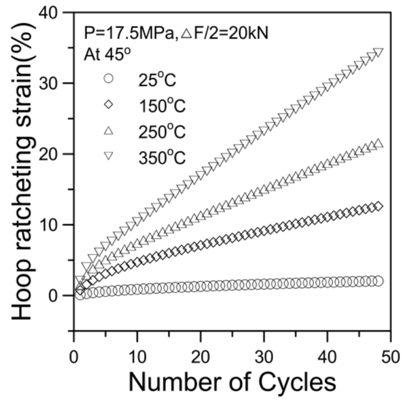


(b) 45°position

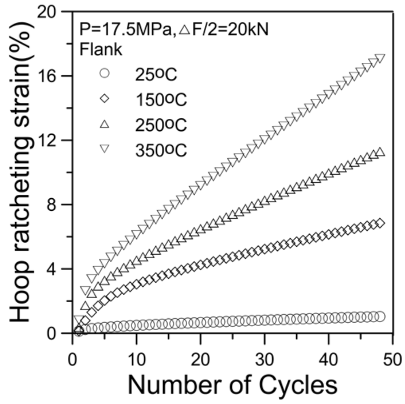


(c) At flank

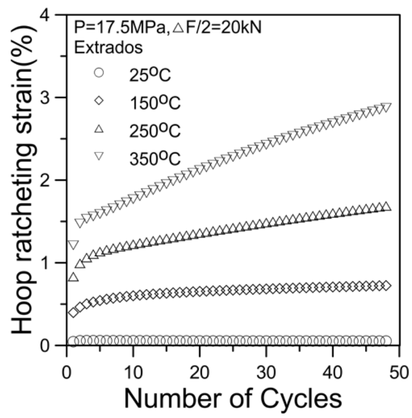


(d) At extrados

Fig. 17 Ratcheting strain at different position under different temperatures

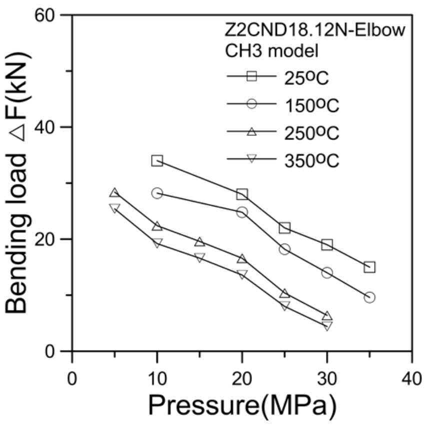

(a) Ratcheting boundary curve

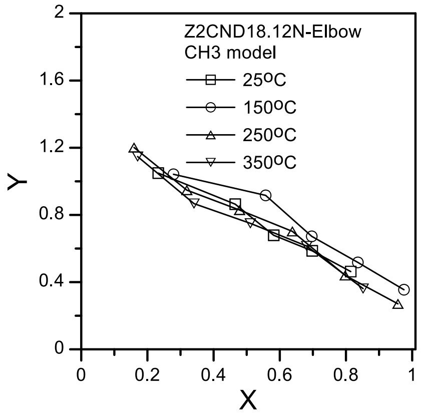

(b) Dimensionless form of ratcheting boundary

Fig. 18 Ratcheting boundary of pressurized elbow pipe subjected to cyclic bending loading under different temperatures

where, $L_s$ was the distance from the bending loading point to the connecting section of straight pipe and elbow pipe, namely the moment arm of nominal bending loading. $\theta$ was the angle of elbow pipe.

The ratcheting boundary of pressurized 90 ° elbow pipe subjected to constant internal pressure and reversed bending was shown in Fig. 18 in which all data were also transformed into $X$ and $Y$ by Eqs. (9) and (11).

It was shown in Fig. 18(a) that reversed bending decreased with the increase of temperature at the same internal pressure, which may be attributed to the relationship of basic characteristics of the materials such as yield strength and the temperature. The dimensionless form of ratcheting boundary was given in Fig. 18(b). Ratcheting boundary under different temperature was not affected by the temperature. In other words, it indicated that ratcheting boundary of 90° elbow pipe and the temperature did not have s relationship.

Moreover, ratcheting boundary of 90° elbow piping subjected to internal pressure and reversed bending was determined by Chaboche model combined with C-TDF method. The results indicated that there is no relationship between the dimensionless form of ratcheting boundary and temperature.

## 7. Conclusions

Austenitic stainless steel Z2CND18.12N used in the auxiliary piping of the primary coolant circuit for pressurized water reactor was studied in this paper. Uniaxial tension and ratcheting tests at 25℃, 150℃, 250℃ and 350℃ were conducted on the Letry electro-hydraulic servo fatigue test machine. Experimental results indicated that elastic modulus, tangent modulus and yield stress decreased with the increase of temperatures. Uniaxial ratcheting decreased with the increase of temperature.

Ratcheting behavior at room temperature of 90° elbow piping subject to internal pressure 20 MPa and reversed bending 20 kN was carried out in test machine. Results indicated that the maximum ratcheting strain occurred in the circumferential direction of 90° elbow piping. Ratcheting strain at flanks and intrados was also very large. The maximum ratcheting strain occurred in the circumferential direction of intrados.

Ratcheting behavior of 90° elbow piping under 150℃, 250℃ and 350℃ was simulated by elastic-plastic finite element analysis combined with Chaboche model. The parameters of Chaboche model were determined based on experimental data of uniaxial tension curve and uniaxial ratcheting strain of the material under 25℃, 150℃, 250℃ and 350℃. For outside surface of elbow piping, it was found that ratcheting behavior at flanks, intrados, extrados and 45° position at midway between flank and intrados occurred. The effect of temperature on ratcheting strain of 90° elbow piping was evident. Ratcheting strain of 90° elbow piping increased with the increase of temperature. Moreover, ratcheting boundary of 90° elbow piping subjected to internal pressure and reversed bending was determined by Chaboche model combined with C-TDF method. The results indicated that there is no relationship between the dimensionless form of ratcheting boundary and temperature.

## Acknowledgments

The authors gratefully acknowledge financial support for this work from the Doctoral Scientific Research Foundation of Liaoning Province (No.201601017), Fundamental Research Funds for the Central Universities (Grant No. N162303001), Youth Foundation of Hebei Educational committee (No. QN2015336), National Natural Science Foundation of China (No. 51435012). The authors acknowledge China Scholarship Council (CSC) which has supplied funding for us to undertake collaborative research. Dr. Haofeng Chen at University of Strathclyde is acknowledged for the assistance of this paper.

## References

Armstrong, P.J. and Frederick, C.O. (2007), “A mathematical representation of the multiaxial bauschinger effect”, *Mater. High Temp.*, **24**(1), 1-26.

Asada, S., Yamashita, N., Okamoto, A. and Nishiguchi, I. (2002), “Verification of alternative criteria for shakedown evaluation using flat head vessel", ASME PVP, 439:17-23.

Bhandari, S., Fortmann, M., Grueter, L., Heliot, J., Meyer, P., Percie du Sert, B. and Zeibig, H. (1986). "Crack propagation in a LMFBR elbow", *Nucl. Eng. Des.*, **91**(2), 107-119.

Chaboche, J.L. (1986), "Time independent constitutive theories for cyclic plasticity", *Int. J. Plasticity*, **2**, 149-188.

Chaboche, J.L., Dang-Van, K. and Cordier, G. (1979), "Modelization of the strain memory effect on the cyclic hardening of 316 stainless steel", *Proceedings of the 5th International Conference on Stuctural Mechanics in Reactor Technology (SMiRT)*, Division L, Berlin, Germany, August.

Chen, X., Gao, B. and Chen, G. (2005), "Multiaxial ratcheting of pressurized elbows subjected to reversed in-plane bending", *J. Pres. Eq. Syst.*, **3**, 38-44.

Chen, X., Gao, B. and Chen, G. (2006), "Ratcheting study of pressurized elbows subjected to reversed in-plane bending", *J. Press. Vess.-T ASME*, **128**:525-32.

Chen, X.H. and Chen, X. (2016), "Effect of local wall thinning on ratcheting behavior of pressurized 90° elbow pipe under reversed bending using finite element analysis", *Steel Compos. Struct.*, **20**(4), 931-950.

Chen, X.H., Chen, X., Chen, G. and Li, D.M. (2015), "Ratcheting behavior of pressurized Z2CND18.12N stainless steel pipe under different control modes", *Steel Compos. Struct.*, **18**(1), 29-50.

Chen, X.H., Chen, X., Yu, D.J. and Gao, B.J. (2013), "Recent progresses in experimental investigation and finite element analysis of ratcheting in pressurized piping", *Int. J. Pres. Ves. Pip.*, **101**,113-142.

Chen, X.H., Chen, X., Yu, W.W. and Li, D.M. (2016), "Ratcheting behavior of pressurized 90° elbow piping subjected to reversed in-plane bending with a combined hardening model", *Int. J. Pres. Ves. Pip.*, **137**, 28-37.

Chen, X., Jiao, R. and Kim, K.S. (2005), "On the ohno–wang kinematic hardening rules for multiaxial ratcheting modeling of medium carbon steel", *Int. J. Plasticity*, **21**(1), 161-184.

Goyal, S., Gupta, S.K., Bhasin, V., Vaze, K.K., Ghosh, A.K., Vishnuvardhan, S., Saravanan, M., Pukazhendhi, DM., Gandhi, P. and Raghav, G. (2010), "Fatigue Ratcheting Investigation on Pressurised Elbows made of SS304 LN", *International Conference on Theoretical, Applied, Computational and Experimental Mechanics*, Kharagpur, India, December.

Griffith, W.I. and Rodabaugh, E.C. (1975), "Tests at room temperature and 1100 F on a 4" Sch. 10 elbow-pipe assembly subjected to in-plane moment loading", *Second National Congress on Pressure Vessels and Piping*, San Francisco, Americal, June.

Gudur, S. (2013), "Fatigue-ratcheting analysis of a pressurized elbow", *Int. J. Recent Adv. Mech. Eng.*, **2**(3), 29-36.

Fenton, M.A. (2015), "Low-cycle fatigue failure and ratcheting responses of short and long radius elbows at room and high temperatures", Master thesis, North Carolina State University, Raleigh, North Carolina.

Hassan, T., Rahman, M. and Bari, S. (2015), "Low-cycle fatigue and ratcheting responses of elbow piping components", *J. Press. Vess.- T. ASME*, **137**, 031010-031010-12.

Hassan, T. and Rahman M. (2015), "Constitutive models in simulating low-cycle fatigue and ratcheting responses of elbow", *J. Press. Vess.- T. ASME*, **137**, 031002-031002-12.

Heald, J.D. and Kiss, E. (1974), "Low cycle fatigue of nuclear pipe components", *J. Press. Vessel Technol.*, **96**(3), 171-176.

Hilsenkopf, P., Boneh, B. and Sollogoub, P. (1988), "Experimental study of behavior and functional capability ferritic steel elbows and austenitic stainless steel elbows", *Int. J. Pres. Ves. Pip.*, **33**(2), 111-128.

Imazu, A., Miura, R., Nakamura, K., Nagata, T. and Okabayashi, K. (1977), "Elevated temperature elastic-plastic-creep test of an elbow subjected to in-plane moment loading", *J. Press. Vess.- T. ASME*, **99**(2): 291-297.

Karamanos, S.A. (2016), "Mechanical behavior of steel pipe bends; an overview", *J. Press. Vess.- T. ASME*, **138**(4): 041203.

Lemaitre, J. and Chaboche, J.L. (1994), "Mechanics of Solid Materials", Cambridge University Press, Cambridge, 1994.

Shi, H.R., Chen, G., Wang, Y. and Chen, X. (2013), "Ratcheting behavior of pressurized elbow pipe with local wall thinning", *Int. J. Pres. Ves. Pip.*, **102- 103**, 14-23.

Ueda, M., Kano, T. and Yoshitoshi, A. (1990), "Thermal Ratcheting Criteria and Behavior of Piping Elbows", *J. Press. Vess.- T. ASME*, **112**(1), 71-75.

Varelis, G.E., Karamanos, S.A. and Gresnigt, A.M. (2013), "Pipe elbows under strong cyclic loading", *J. Press. Vess.- T. ASME*, **135**(1), 011207-1-9.

Varelis, G.E. and Karamanos, S.A. (2014), "Low-cycle fatigue of pressurized steel elbows under in-plane bending", *J. Press. Vess.- T. ASME*, **137**(1), 011401-1-10.

Yahiaoui, K., Moreton, D.N. and Moffat, D.G. (1996), "Response and cyclic strain accumulation of pressurized piping elbows under dynamic out-of-plane bending", *J. Strain Anal. Eng. Des.*, **31**, 153-166.

Yamamoto, Y., Yamashita, N. and Tanaka, M. (2002), "Evaluation of thermal stress ratchet in plastic FEA", *ASME PVP*, **439**:3-10.

Zakavi, S.J., Ajri, M. and Golshan V. (2014), "The ratcheting behaviour of plain carbon steel pressurized piping elbows subjected to simulated seismic in-plane bending", *World J. Mech.*, **4**, 238-246.

Zakavi, S.J. and Nourbakhsh M. (2014), "The ratcheting behaviour of stainless steel pressurized piping elbows subjected to dynamic out-of-plane moments", *Mod. Mech. Eng.*, **4**, 125-132.

*CC*